INTERFEROMETRIC PROCESSING ALGORITHMS OF TANDEM-X DATA

Nestor Yague-Martinez[1], Cristian Rossi[1], Marie Lachaise[1], Fernando Rodriguez-Gonzalez[2], Thomas Fritz[1], Helko Breit[1]

[1]German Aerospace Center, (DLR), Remote Sensing Technology Institute,82234 Wessling, Germany
[2]Technische Universität München, Remote Sensing Technology, Arcisstr. 21, 80333 Munich, Germany

ABSTRACT

The purpose of this paper is to provide an algorithmic overview of the interferometric processing embedded in the Integrated TanDEM-X Processor (ITP), settled to the generation of the raw digital elevation model (DEM). The main processing blocks are described, with a focus on the spectral matching of the azimuth spectra, the high-precision coregistration, the dual-baseline phase unwrapping and the geocoding of the products. The robustness of the algorithms is demonstrated through a dual-pass TerraSAR-X scenario.

Index Terms— TanDEM-X, InSAR, SAR, ITP

1. INTRODUCTION

The German TanDEM-X mission, started on the 21st June, 2010, is based on two TerraSAR-X satellites flying in close formation and establishing the first bistatic single pass interferometer in space. The primary objective of the mission is the generation of a consistent global digital elevation model (DEM) with an unprecedented accuracy, which is equaling or surpassing the HRTI-3 specification [1]. Systematic processing of SAR raw data to so-called raw DEMs is performed by one single processing system, the Integrated TanDEM-X Processor (ITP). The final global DEM is then calibrated and mosaicked. In this paper an overview of the InSAR algorithms of ITP is presented.

2. ALGORITHMIC OVERVIEW

The interferometric processing chain of the ITP [2] is composed of five main processing blocks, as shown in Figure 1. After the SAR focusing chain, master and slave Single look Slant range Complex (SSC) data are filtered to their common spectrum (Sec. 2.1) and coregistered (Sec. 2.2), for the generation of the interferogram. A single or dual phase unwrapping operation is then performed, according to the mission planning (Sec. 2.3). Finally, a raw DEM and a set of files assessing the quality and the geometric properties of the scene are generated as output (Sec. 4). The coregistered master and slave data (CoSSC), used as a support of the dual baseline phase unwrapping, are also provided.

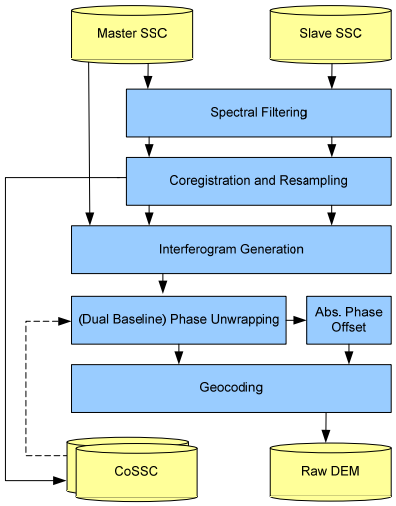

Figure 1: High level block scheme of the interferometric processing chain embedded in ITP. The internal interfaces are not shown for clarity.

2.1 Spectral filtering

Due to the different acquisition geometries, master and slave received spectra are composed of a coherent and a non-coherent band, both in range and azimuth. In order to simultaneously increase the coregistration precision [3] and reduce the variance of the final height estimate [4], the non-coherent bands should be eliminated. Figure 2 shows the coherence loss due to the range non-coherent band, effect known as geometric decorrelation.
In azimuth the overlapping bands are derived from Doppler Centroid estimates and the azimuth processing bandwidth. In range the relative shift between the coherent bands is estimated from a phase simulation based on the ellipsoid corrected with the mean height of the scene.
A filter that selects only the common bands is used. In azimuth its parameters are adapted on a line-by-line basis and processing is performed block-wise, updating the filter twice a second in order to follow the azimuth variations of the Doppler Centroids. These are caused by the satellites' short term attitude variations. Filtering in range can be processed block-wise in order to follow the fringe frequency variation of the simulation. The final configuration will be determined during the Commissioning Phase.

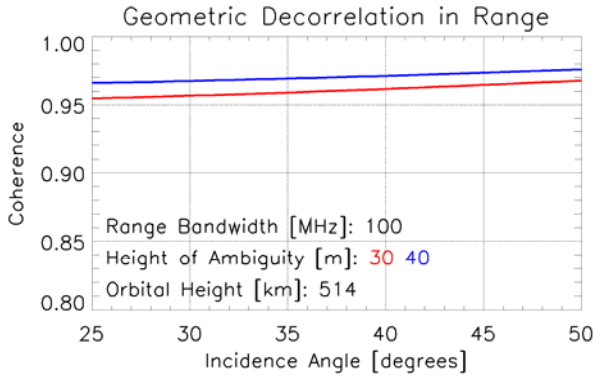

Figure 2: Coherence variation in a TanDEM-X scenario for the first year of full coverage (blue) and the second year (red). The gain obtained with a range spectral filtering is of about 3% - 5%.

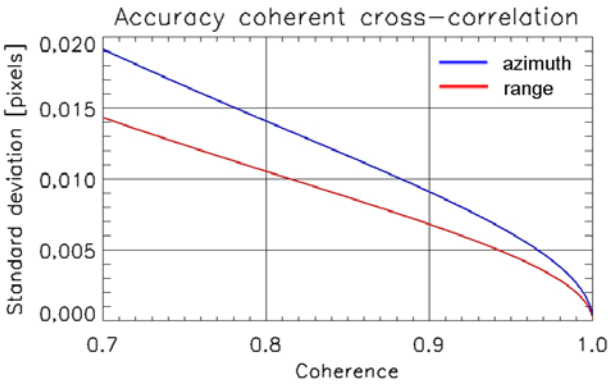

Figure 3: Accuracy with coherent cross-correlation for range and azimuth directions. N=1024; Range osf = 1.1; Azimuth osf = 1.35

2.2 Coregistration and Resampling

SAR image coregistration is an operation which obtains a precise overlap between two or more SAR images relative to the same object. Such images are usually acquired from separated positions. Because of the high resolution of the system and the terrain dependent distortions, coregistration polynomials are not appropriate. Instead mapping matrices are generated and used for coregistration. The coregistration algorithm is structured in the following steps [3]:

- *Geometrical coregistration*

A geometrical calculation on a regular grid of the range and azimuth shifts of the slave scene with respect to the master scene is performed. An external DEM and precise orbit information of master and slave satellites are used as input information.

- *Cross-Correlation*

Cross-correlation operation is performed with patches arranged on the grid. The a-priori estimates coming from the geometrical coregistration are used to extract these patches from the slave scene. Thus the overlapping area of the patches can be maximized. Cross-correlation is performed in its two variants: coherent (i.e. using the *complex* image samples), which is the optimum (maximum likelihood) estimator for differential shift of partially correlated circular Gaussian signals[7], but which is very sensitive to phase differences between both patches because of e.g. topographic fringes. The second variant is the incoherent cross-correlation (correlates only with the intensity of the image patches), which is a suboptimum estimator, but more robust than the coherent version.

Coherent cross-correlation is firstly calculated. A simulated topographical phase is removed in order to compensate the phase cycles due to the topography. A peak test of the correlation function is then done, if it is not passed, the coherent cross-correlation function is discarded and incoherent cross-correlation is applied. A peak-test is also performed for this last function.

- *Outliers elimination*

An outlier elimination procedure of the resampling matrices based on the correlation coefficient and on the shift values is performed.

The Slave image is finally resampled on the master grid using the mapping matrices previously estimated. This operation is performed in time domain in order to locally follow the shifts patterns.

2.2.1. Coregistration accuracy

According to [7], the displacement accuracy using coherent cross-correlation is given by the Cramer-Rao bound:

$$\sigma_{cc} = \sqrt{\frac{3}{2 \cdot N}} \frac{\sqrt{1-|\gamma|^2}}{\pi \cdot |\gamma|} \cdot osf^{\frac{3}{2}}$$

being, N the number of pixels of the correlation patch; *osf* the oversampling factor and γ the coherence.

Some experiments have been performed with dual-pass TerraSAR-X data using 32 x 32 pixels patches. This patch size results in an enough precision for interferogram generation, as shown in Figure 3.

It is not aware of an analytical expression for the estimation error of incoherent cross-correlation. The accuracy of the method depends on the presence of coherent speckle or features in the patches. In the case of homogeneous patches and high coherence values, the error should be a factor $\sqrt{2}$ larger than that for the coherent case.

Some coregistration results with dual-pass TerraSAR-X data are presented. Patches are separated by a distance of 100 pixels in both directions.

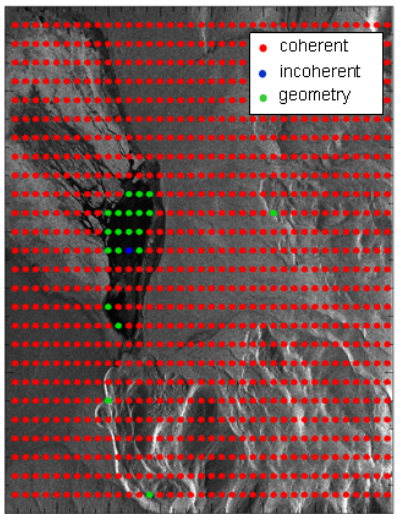

Figure 4: Overlay of the SAR Amplitude and the correlation type map. Red points correspond to coherent cross-correlation; blue points to incoherent cross-correlation; green points represent patches where neither coherent nor incoherent correlation worked. A geometric estimate substitutes these points.

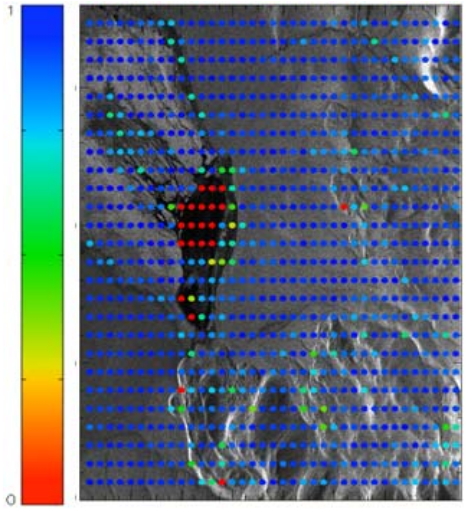

Figure 5: Overlay of the SAR Amplitude and the correlation coefficient map.

Figure 4 shows an overlay of the SAR amplitude and the cross-correlation type map. The correlation coefficient map is presented in Figure 5.
It can be observed here that the patches, where coherent cross-correlation has not worked and then incoherent cross-correlation has been worked represent a small percentage of the total of patches (only areas with low backscattering or where the topographic phase could not be rightly compensated).

2.3 Single and dual baseline Phase Unwrapping

The purpose of phase unwrapping is to recover the absolute phase given the ambiguous wrapped interferometric phase. It constitutes the critical step in the interferometric chain.
The terrain height difference corresponding to a phase variation of one cycle is the so-called height of ambiguity and depends directly on the baseline. The smaller the height of ambiguity, the greater the phase difference between two points and the more difficult the unwrapping process. On the contrary, a larger height of ambiguity implies that fringes are easier to unwrap,nevertheless with poorer topography accuracy. The TanDEM-X acquisition plan has been designed from this approach, i.e. a first acquisition stage with a large height of ambiguity (ca. 40 – 50 m/cycle), and a second one with a smaller one (ca. 25 – 35 m/cycle).
The interferograms obtained with the larger height of ambiguity are unwrapped using the Minimum Cost Flow (MCF) algorithm [5], which was used successfully during the SRTM mission. Once interferograms with the smaller height of ambiguity will be available, a new approach which combines MCF and Maximum A Posteriori (MAP) will be used [6]. In this case, MAP is first used to reduce phase gradient ambiguities. Then, phase unwrapping of the most accurate interferogram is performed with the MCF algorithm using the gradient estimates obtained previously. In this way, since ambiguities have been mostly solved, single baseline phase unwrapping is notably enhanced, helping many of its difficulties.

A datatake is splitted in scenes of about 50km (along-track) by 30km (across-track), for which an independent processing is performed. To ensure a continuity of the digital elevation model along the datatake, without gaps or offset between the scenes, a constant phase is added to the unwrapped one for every scene ("absolute phase offset"). This value is estimated using a simulated interferogram from an external DEM.

2.4 Geocoding

The final step is the generation of the raw DEM starting from the interferometric unwrapped phase, also known as *geocoding*. It involves the conversion to terrain height and the transformation from slant-range coordinates to an Earth-related reference frame. The key concept is to find the intersection between two curves:

- The interferometric phase $\Phi(r)$, which has a monotonous (decreasing or increasing) behaviour as a function of range time.
- The geometric phase $\varphi(r)$, linking the interferometric phase to the height of one object on the earth. This phase can be related to range time, as a vertical straight line of increasing terrain height crosses the circles of constant range delays, and it is monotonous as well, with a trend opposite to $\Phi(r)$, intersecting thus the first one.

This concept allows in a single step to obtain the output desired, since it links all the parameters involved for geocoding: azimuth and range times, interferometric phase and terrain height. $\varphi(r)$ is computed for every point of the desired output grid through an inverse geocoding relating different terrain height to the satellite positions (master and slave). During the processing the signal delay is corrected for the tropospheric / ionospheric path, increasing the final geometrical accuracy. Moreover, a set of quality maps is generated [4].

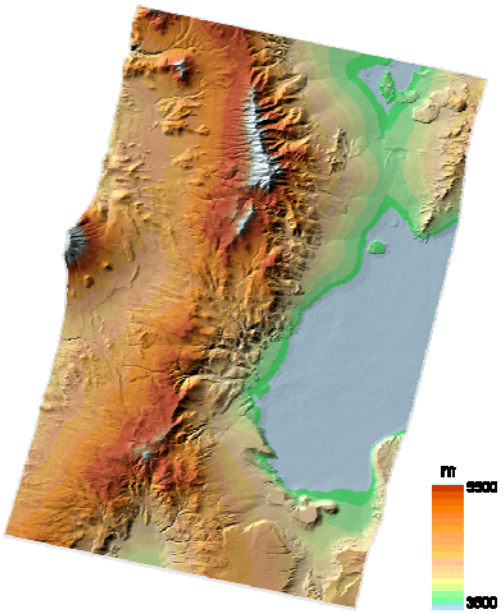

Figure 6: Example of Raw DEM generated by ITP. The processing of this scene revealed a low percentage of layover areas (0.2%) and of shadow areas (0.05%).

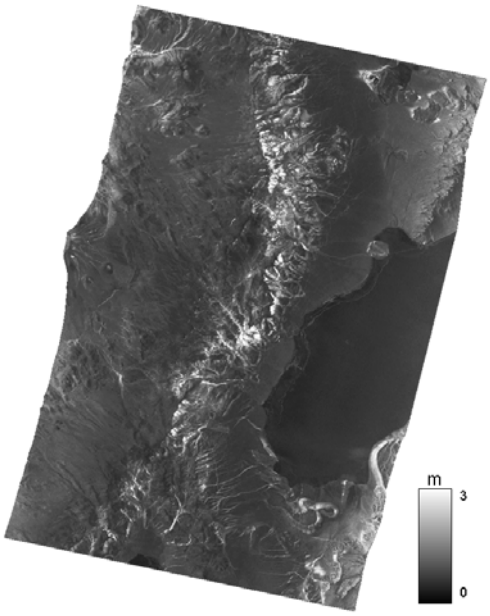

Figure 7: Height Error Map for the raw DEM in Figure 6. The high coherence (mean 0.89) yields a mean error of 0.65 meters.

3. PROCESSING RESULTS

At the submission of this paper, only dual-pass TerraSAR-X data was available. A 1-cycle (11 days) interferometric pair in a mountainous region of Chile with high coherence (mean 0.89) was chosen as test site.

Figure 6 shows the output of the chain, the raw DEM. The DEM grid spacing for this area is defined as 0.2 arc-seconds for both latitude and longitude. A quality map generated by the processor is the *Height Error Map*, representing, for each pixel, the standard error of the corresponding elevation value in the DEM. Figure 7 shows this map for the raw DEM in Figure 6.

4. CONCLUSIONS

The second TerraSAR-X satellite (TD-X) has been launched on the 21st June 2010. Since the 24th June numerous test images in several modes and polarizations have been successfully acquired and processed. At the submission date of the paper the Pursuit Monostatic Commissioning Phase had not started. Therefore the algorithms described have not yet been tested with the tandem configuration, which will avoid the limitations due to temporal decorrelation and atmospheric delay. Nevertheless their geometrical accuracy and robustness has been demonstrated with several dual-pass TerraSAR-X scenario.

4. REFERENCES

[1] G. Krieger, A. Moreira, H. Fiedler, I. Hajnsek, M. Werner, M. Younis and M. Zink. *TanDEM-X: A satellite formation for High-Resolution SAR Interferometry*, TGARS, Vol 45, No 11. November 2007

[2] T. Fritz, H. Breit, U. Balss, N. Yague-Martinez, C. Rossi, A. Niedermeier, M. Lachaise, F. Rodriguez-Gonzalez. *Processing of Interferometric TanDEM-X Data*. EUSAR 2010

[3] N. Yague-Martinez, M. Eineder, H. Breit, T. Fritz, R. Brcic. *TanDEM-X Mission: SAR Image Coregistration Aspects*. EUSAR 2010

[4] C. Rossi, M. Eineder, T. Fritz, H. Breit. *TanDEM-X Mission: Raw DEM Generation.* EUSAR 2010

[5] M. Eineder, M. Hubig, and B. Milcke, *Unwrapping large interferograms using the minimum cost flow algorithm*. Geoscience and Remote Sensing Symposium Proceedings. IEEE, 1998, pp. 83–87.

[6] M. Lachaise, F. Rodriguez Gonzalez, R. Bamler, *Multibaseline gradient ambiguity resolution to support Minimum Cost Flow phase unwrapping.* IGARSS 2010.

[7] R. Bamler. *Interferometric stereo radargrammetry: Absolute height determination from ERS-ENVISAT interferograms, in Proc. IGARSS, vol. 2, July 2000, pp 742 – 745.*